International Journal of Nanomedicine

Dovepress
open access to scientific and medical research

Open Access Full Text Article

ORIGINAL RESEARCH

Influence of GO-Antisense miRNA-21 on the Expression of Selected Cytokines at Glioblastoma Cell Lines

Marta Kutwin[1], Malwina Sosnowska[1], Agnieszka Ostrowska[1], Maciej Trzaskowski[2], Agata Lange[1], Mateusz Wierzbicki[1], Sławomir Jaworski[1]

[1]Department of Nanobiotechnology, Institute of Biology, Warsaw University of Life Sciences, Warsaw, 02-786, Poland; [2]Centre for Advanced Materials and Technologies CEZAMAT, Warsaw University of Technology, Warsaw, 02-822, Poland

Correspondence: Marta Kutwin, Department of Nanobiotechnology, Institute of Biology, Warsaw University of Life Sciences, 8 Ciszewskiego street, Warsaw, 02-786, Poland, Tel +48-225936671, Email marta_kutwin@sggw.edu.pl

Introduction: Graphene oxide (GO) is a single layer of carbon atoms with unique properties, which are beneficial due to its surface functionalisation by miRNA. miRNAs are a non-coding small form of RNA that suppress the expression of protein-coding genes by translational repression or degradation of messenger RNA. Antisense miRNA-21 is very promising for future investigation in cancer therapy. This study aimed to detect cytokine expression levels after the administration of GO-antisense miRNA-21 into U87, U118, U251 and T98 glioma cell lines.

Methods: U87, U118, U251 and T98 glioma cell line were investigated in term of viability, human cytokine expression level at protein and genes after treatment with GO, GO-antisense miRNA-21 and antisense miRNA-21. The delivery of antisense miRNA-21 into the glioma cell at in vitro investigation were conducted by GO based transfection and electroporation.

Results: The results of the protein microarray and gene expression profile showed that complexes of GO-antisense miRNA-21 modified the metallopeptidase inhibitor 2 (TIMP-2), interleukin-6 (IL-6), interleukin 8 (IL-8), intercellular adhesion molecule 1 (ICAM-1), and monocyte chemoattractant protein-1 (MCP-1) expression level compared to transfection by electroporation of antisense miRNA-21 at investigated glioblastoma cell lines. The TIMP-2 protein and gene expression level was upregulated after antisense miRNA-21 delivery by GO complex into U87, U251 and T98 glioblastoma cell lines comparing to the non-treated control group. The downregulation at protein expression level of ICAM – 1 was observed at U87, U118, U251 and T98 glioma cell lines. Moreover, the IL-8 expression level at mRNA for genes and protein was decreased significantly after delivery the antisense-miRNA-21 by GO compared to electroporation as a transfection method.

Discussion: This work demonstrated that the graphene oxide complexes with antisense miRNA-21 can effectively modulate the cytokine mRNA and protein expression level at U87, U118, U251 and T98 glioma cell lines.

Keywords: graphene oxide, miRNA-21, cancer, miRNA delivery, glioblastoma

Introduction

The goal of gene cancer therapy, also known as gene therapy for cancer, is to either destroy cancer cells directly or to make them more susceptible to other types of cancer treatment, such as chemotherapy or radiation therapy. One of the most promising gene therapy approaches for glioma is the use of viral vectors to deliver therapeutic genes to cancer cells and increase the efficiency of chemotherapy and immunotherapy for cancer.[1] Viral vectors are genetically engineered viruses that can infect and deliver genes to specific cells, including cancer cells. The effectiveness varies depending on the specific type of cancer and the stage of the disease.[2] However, the delivery of miRNA by viral vectors is also associated with potential side effects, including uncontrolled immune response, cytotoxicity, limited efficiency, and rare but possible off-target effect.[3] Alternatively, non-viral vectors can be applied in gene therapy for cancer, and generally, these non-viral vectors are safer than viral ones as they do not pose the same risks of immune response and toxicity. One

Received: 4 May 2023
Accepted: 24 July 2023
Published: 28 August 2023

idea for dealing with the side effects of viral vectors for gene delivery is the usage of nanoparticles to improve gene transport by protecting the genetic material from degradation in the bloodstream, facilitating its uptake by cells, and targeting specific tissues or cell types.[4] Nanoparticles can be engineered to carry and deliver genetic material to specific cells or tissues. They can protect the genetic material from degradation by enzymes in the bloodstream and can be modified to release the genetic material once they reach the target cells, thus enhancing the efficiency of gene delivery. Additionally, nanoparticles can be designed to release genetic material in response to specific stimuli, such as changes in pH or temperature, which can further improve their specificity and efficiency. Moreover, carbon nanoparticles can be engineered to fuse with the cell membrane, allowing the genetic material to enter the cell.[5] Gene delivery, such as electroporation, uses an electric field to temporarily create pores in the cell membrane, allowing the genetic material to enter the cell more easily. Carbon nanomaterials have unique physiochemical properties that make them highly desirable for a wide range of applications, including electronics,[5] energy storage,[6] biomedical engineering,[7] and environmental remediation.[8] One form of carbon nanomaterial is graphene oxide (GO) which is a two-dimensional sp2-hybridised bond of carbon and oxygen atoms arranged in a carbon hexagonal pattern. Its physicochemical features, including thickness, stiffness, unique electrochemical properties, high thermal conductivity, optical transmittance, and very high hydrophobicity, are still being intensively studied.[9] The analysis of the in vivo entry patch of GO indicated that GO could reach different locations through blood circulation or biological barriers, resulting in varying degrees of retention in different organs. The size duality of the nanometric scale showed that GO can reach deeper organs by passing through the normal physiological barriers, such as the blood-air barrier, blood-testis barrier, blood-brain barrier and blood-placental barrier. Graphene nanomaterials with an average diameter of 342 ± 23.5 nm, decreased the blood-brain barrier paracellular tightness and soaked through the paracellular pathway into the inter-endothelial cleft in a time-dependent manner.[10] The 2D structure and surface group of GO which include hydroxyl (-OH), epoxy (-O-), and carboxyl (-COOH) groups are most beneficial for life science applications due to its specific monolayer surface area, which can be successfully loaded by DNA or RNA.[11] The presence of these functional groups makes GO hydrophilic and allow it to interact with water and other polar solvents, making it easier to disperse in aqueous solutions. GO has emerged as a promising nanocarrier for drug delivery due to its unique physical, chemical, and biological properties. GO at size range between 800–1200 d. nm[12] as a miRNA carrier, can be used to protect miRNAs from degradation and facilitate their uptake by cancer cells. GO-miRNA complexes at size 805.0 d. nm (PDI = 0.305) can be efficiently internalised by glioma cancer cells via endocytosis and then released into the cytoplasm.[12] Once in the cytoplasm, the miRNAs can exert their regulatory functions by binding to target mRNAs and repressing their translation or inducing their degradation.[3] In addition to protecting miRNAs from degradation and facilitating their uptake by cancer cells, graphene oxide also offers other advantages as a drug delivery platform, including low toxicity, biocompatibility, and the ability to be functionalised with targeting ligands to selectively deliver drugs to cancer cells.[13] Published data have already shown that GO can cross cell membranes,[14] presents a high affinity to the cell body,[15] interacts with genetic materials[16] and nuclei[17] and accumulates at the site of administration.[18]

In cancer, miRNAs are often deregulated, meaning that their expression levels are altered compared to normal tissues.[3] This deregulation can contribute to the development and progression of cancer by promoting cell proliferation, migration, invasion, and resistance to apoptosis while inhibiting cell differentiation and apoptosis. In this study, we investigated the four different glioma cell lines that exhibit genetic, morphological, and metabolic variations, although they are all derived from non-primary sources. Vogel et al[19] also conducted an analysis of U87, U118, U251, and U117 GBM cell lines, revealing that each cell line expressed a small number of unique proteins (5–10 proteins), while there was a significantly higher number of shared proteins (>100 proteins) between each cell lines. The difference at the protein expression level impacts metabolic activity and drug efflux, affecting the cellular response to anticancer treatments. For example, miRNA-21 is upregulated in glioblastoma and is known to promote cancer cell proliferation, migration, and invasion.[20] Additionally, Aloizou et al[20] published data demonstrated differences between miRNA-21 expression levels, glioma grade, and the U87, U118, U251 GBM cell lines, showing a strong correlation between the high grade and high expression of miRNA-21 at GBM samples. MiRNA-21 has been found to regulate the expression of other cytokines, such as transforming growth factor beta (TGF-β), which is a potent immunosuppressive cytokine that promotes tumour growth and metastasis. Cytokines are signalling molecules that play important roles in immune

regulation and inflammation, and their dysregulation is often associated with cancer development and progression. For example, miRNA-21 has been found to target the NF-κB pathway, which is a key regulator of cytokine production, including interleukin-6 (IL-6), tumour necrosis factor-alpha (TNF-α), and interleukin-1beta (IL-1β).[21] By inhibiting NF-κB signalling, miRNA-21 can reduce the expression of cytokines and potentially modulate the inflammatory response in cancer cells by targeting the TGF-β signalling pathway.[22] Moreover, miRNA-21 can regulate the expression of extracellular matrix proteins like the TIMP protein family by targeting its mRNA. Specifically, miRNA-21 binds to the 3' untranslated region (UTR) of STAT protein mRNA and inhibits its translation, leading to a decrease in TIMP-2 protein expression.[23] In cancer, miRNA-21 overexpression has been associated with increased MMP protein activity, which promotes tumour invasion and metastasis.[24] To silence the overexpression of miRNA-21 in glioblastoma, antisense miRNA-21 can be administered into cancer cells, leading to the inhibition of miRNA-21 function and the restoration of normal gene expression.[12] Antisense miRNA is a type of RNA molecule that is complementary to a specific miRNA molecule. It is designed to hybridise with and bind to miRNA, preventing it from binding to its target mRNAs and inhibiting their translation. Restoring normal miRNA expression levels in cancer cells is a promising strategy for cancer therapy. Antisense miRNA-21 can inhibit the expression level of miRNA-21 and increase the expression of PTEN, a tumour suppressor gene, and decrease cytokine expression levels, especially IL-6 and TNF-α.[25] Inhibition of miR-21 has been shown to suppress glioblastoma growth and invasion in preclinical studies.[12] Several studies have reported the successful delivery of antisense miRNA-21 using GO in various cancer models, including breast, lung, and colon cancer.[25,26] GO can be functionalised with antisense miRNA by chemically conjugating or adsorbing the antisense miRNA onto the surface of GO. Chemical conjugation involves covalent bonding between the antisense miRNA and GO, which can be achieved through various chemical reactions or click chemistry. This method allows for stable attachment of the antisense miRNA to GO, preventing detachment or degradation during delivery.[27] Adsorption involves non-covalent bonding between the antisense miRNA and GO, which can be achieved through electrostatic interactions or π-π stacking. This method is simpler and faster than chemical conjugation, but the attachment of the antisense miRNA to GO may not be as stable or controlled as with chemical conjugation.[12] Functionalizing GO with antisense miRNA allows for the specific delivery of antisense miRNA to target cells and downregulation of the targeted mRNA, which can lead to changes in the expression of proteins. GO can be functionalised with polyethylene glycol (PEG) and conjugated with antisense miRNA-21 to form a stable and biocompatible nanocomplex for effective inhibition of miRNA-21 function and for suppressing the growth of cancer cells in vitro and in vivo.[25] In another study, GO was functionalised with chitosan and conjugated with antisense miRNA-21 to form a stable and biocompatible nanocomplex for the treatment of lung cancer cells to suppress their growth and invasion.[28] GO has been shown to regulate cytokine protein expression[29] in glioblastoma by delivering therapeutic agents that target specific cytokines or cytokine pathways.[30] GO in glioma cells also regulated the protein expression level of IL-6, IL-8, and MCP-1 by the activation of the NF-κB signaling pathway.[31] The downregulation of IL-6 and Il-8 was also correlated with decreased levels of angiogenesis in glioma in an in ovo cancer model.[31] GO is a promising nanomaterial for delivering antisense miRNA-21 to glioma cancer cells, leading to the inhibition of selected protein functions. However, more research is needed to optimize the delivery of GO-based nanocomplexes and evaluate their safety and efficacy. Therefore, this study aimed to assess the potential effects of complexes of graphene oxide-antisense miRNA-21 vs electroporation with antisense miRNA-21 on cytokine expression levels at the U87, U118, U251, and T98 GBM cell lines. Increasing the knowledge of the possible effects of antisense-miRNA-21 delivery by GO structures will provide important tools to improve GO as a non-viral platform for gene delivery in cancer treatment development.

Methodology

Graphene Oxide (GO) and Complex Graphene Oxide with Antisense miRNA-21 (GO-miRNA-21)

GO colloid (GO) (purity 99.99%) was purchased from Nanopoz (Poznan, Poland) and dispersed in ultrapure water to prepare a 1.0 mg/mL solution. After 30 minutes of sonification, the hydrocolloid of GO was diluted to 100 μg/mL and mixed with antisense miRNA-21 (UAGCUUAUCAGACUGAUGUUGA; HSTUD0399, Sigma-Aldrich, USA) at

a concentration of 5 pmol/mL in ultrapure water and used without additional purification and filtration. Ultrasonic coating of GO nanosheets for 30 minutes took place in a 50 mL glass flask.

Transmission Electron Microscopy

The shape and size of the GO, antisense miRNA-21, and GO-miRNA-21 were inspected using a transmission electron microscope (TEM). The morphology of GO and GO-miRNA-21 was inspected using a transmission electron microscopy (TEM.JEOL JEM-1220, JEOL Ltd., Tokyo, Japan) at 80 KeV equipped with an 11-megapixel camera (Morada TEM, Olympus Corporation, Tokyo, Japan). Triplicate samples of GO and GO-antisense miRNA-21 were prepared for TEM by placing droplets of the hydrocolloid onto Formvar-coated copper grids (Agar Scientific Ltd., Stansted, UK) and air drying before TEM imaging.

Fourier Transform Infrared (FTIR) Spectroscopy

The FTIR spectra of dried samples were recorded using an FTIR spectroscope with a diamond ATR pickup (Nicolet 6700, Thermo Scientific). All samples were prepared by dropping 200 µL of sample suspension on a microscope glass and drying the suspension at 40°C. Each spectrum was rationed to a background spectrum previously registered with an empty measuring chamber. This was done to remove the effect of carbon dioxide and water vapour present in the laboratory air.

Dynamic Light Scattering and ζ-Potentials

Particle sizes were measured in a particle size analyser (Zetasizer ZSP, Malvern Instrument Ltd., Worcestershire, UK) at 25°C based on laser Doppler velocimetry and dynamic light scattering (DLS) techniques. Previously, the suspension was homogenised using an ultrasonication probe for 30 min.

The ζ-potentials of GO, antisense miRNA-21, and GO-antisense miRNA-21 were measured by the dynamic laser scattering electrophoretic method, using the Smoluchowski approximation with a zeta potential analyser (Zetasizer Nano ZS90 Malvern Instruments, Malvern, UK). Each sample was measured after stabilisation at 25°C for 120 s.

All measurements were performed in triplicate.

Entrapment Efficiency

The miRNA entrapment efficiency (EE) of graphene oxide complexes was obtained from the determination of free miRNA concentration in the GO + miRNA supernatant recovered from the centrifugation process. The concentrations were measured using a spectrophotometer (NanoDrop 2000, Thermo Scientific, Wilmington, DE, USA). The concentration of free miRNA was determined using Beer's Law, and calculations were done using the following equation: $C = A/(\varepsilon \times b)$ where A is the concentration of miRNA, ε is the extinction coefficient, and b is the path length of the cuvette. The sample was measured in triplicate.

The entrapment efficiency was calculated by using the following Equation (1):

$$EE = \frac{\text{concentration of miRNA added} - \text{concentration of miRNA in supernatant}}{\text{concentration of miRNA added}} \text{x}100\% \quad (1)$$

Cell Cultures and Treatments

Cell Culture

GBM cell lines U87, U118, U251, and T98 used in this study were obtained from the American Type Culture Collection (Manassas, VA, USA) and maintained in Dulbecco's Modified Eagle's Medium supplemented with 10% foetal bovine serum (Sigma-Aldrich) and 1% penicillin and streptomycin (Sigma-Aldrich) at 37°C in a humidified atmosphere of 5% CO_2/95% air in an air-jacketed CO2 incubator (NuAire DH AutoFlow, Plymouth, MN, USA).

GO-Antisense miRNA-21 Treatment of Glioblastoma

The selection for the concentration of graphene oxide and antisense miRNA-21 was made based on our previously published data.[8] The final concentration for graphene oxide was 100.00 µg/mL, and for antisense miRNA-21 5.00 pmol/

mL. Cells were cultured in 6-well plates (1×10^5 cells per well), and the GO-miRNA-21 at a concentration of $GO_{100\mu g/mL}$: antisense $miRNA\text{-}21_{5pmol/mL}$ was added to each well and incubated for 24h. After incubation, the cells were cultivated in 6-well plates (1×10^5 cells per well) for 24h. Next, the supernatant was removed, and the cells were washed with PBS and incubated in a fresh medium containing 10% FBS for 24h.

Electroporation with Antisense miRNA-21

For transfection by electroporation, the U87, U118, U251, and T98 GBM cells were cultured in a 75 cm^3 flask (9×10^6 cells). After collection, the cells were suspended into 200 µL of electroporation buffer (165–2676, Bio-Rad, Hercules, USA) for a final cell concentration of 1×10^6 and placed in a 0.2 µm electroporation cuvette (165–2092, Bio-Rad). Next, 2 µL of antisense miRNA-21 were introduced into the U87, U118, U251, and T98 cell lines. The electroporation was performed according to previously published data by Kutwin et al.[12]

Cell Morphology and Transfection Efficiency Evaluation After Administration of Graphene Oxide-Antisense miRNA-21 into the U87, U118, U251, and T98 Glioma Cell Lines

The morphology of the U87, U118, U251, and T98 glioma cell lines after transfection or electroporation with GO antisense miRNA-21 ($GO_{100\ \mu g/mL}$: antisense $miRNA\text{-}21_{5\ pmol/mL}$) was investigated. For transfection efficiency evaluation, 0.1 mg of FITC (F143, Thermo Fischer Scientific, Waltham, MA, USA) was used to label the GO, antisense miRNA-21, and complex of GO-antisense miRNA-21 sequences by overnight incubation at 4°C, protected from light. The GO, antisense miRNA-21, and GO-antisense miRNA-21 complex were introduced to the U87, U118, U251, and T98 cell lines by electroporation or transfection, as described in the preceding sections of this manuscript. Cells after transfection and electroporation were placed on glass slides on 6-well plates (1×10^5 cells per well). After 24 h, the cell morphology was observed, and transfection efficiency was evaluated and recorded with an confocal microscope (IX 81 FV-1000, Olympus Corporation, Tokyo, Japan).

Image analysis in confocal mode, Nomarski interference contrast, and cell counting were performed using FVIO-ASW ver. 1.7c software (Olympus Corporation, Tokyo, Japan). Three-dimensional images were assembled from 30 optical sections. All measurements were performed in triplicate.

Cell Viability Assay After Graphene Oxide-Antisense miRNA-21 Administration or Electroporation with Antisense miRNA-21 into Glioma Cells

Cell viability was evaluated using a cell viability assay based on a resazurin-fluorescent dye (PrestoBlue™ Reagent, Life Technologies, Taastrup, Denmark). Metabolic active cells convert the dark blue oxidised form of the dye (resazurin) into a red-fluorescent reduced form (resorufin; λEx = 570 nm; λEm = 590 nm). Cells after transfection with GO-antisense miRNA-21 ($GO_{100\ \mu g/mL}$:$miRNA_{5\ pmol/mL}$) were incubated in 96-well plates (5×10^3 cells per well). Next, the dye solution was added to each well at a 1:10 ratio and then incubated for an additional 2 h at 37°C. The OD of each well was recorded at 570 nm with a 590 nm reference with a scanning multiwell spectrophotometer (Infinite M200, Tecan, Durham, NC, USA). Cell viability was expressed as a percentage (ODtest − ODblank)/(ODcontrol − ODblank), where "ODtest" is the OD of cells exposed to GO and rGO, "ODcontrol" is the OD of the control sample, and "ODblank" is the OD of wells without cancer cells.

Cytokine Expression

Protein Expression Level

Isolation of Total Protein

For protein analysis, glioma cells were treated with GO-antisense miRNA-21. Cells not treated with nanoparticles were used as the control. Whole-cell protein extracts were prepared by suspending cells in an ice-cold radioimmunoprecipitation assay (RIPA) buffer containing protease and phosphatase inhibitors (Sigma-Aldrich, St. Louis, MO, USA). The cells were incubated on ice for 30 min (vortexing at 10 min. intervals) before being centrifuged (30 min; 14,000×g; 4°C), and

the supernatant was collected. The nuclear fraction was obtained by suspending cells in a hypotonic buffer (20 mM Tris-HCl, pH 7.4; 10 mM NaCl; 3 mM $MgCl_2$). Igepal CA-630 (Sigma-Aldrich) containing protease and phosphatase inhibitors (Sigma-Aldrich) was added to a final concentration of 0.5%, and the solution was vortexed for 10s. The pellet containing the nuclear fraction was resuspended in an ice-cold RIPA buffer containing protease and phosphatase inhibitors and incubated on ice for 30 min (vortexing at 10 min. intervals). The supernatant of the nuclear fraction homogenate was collected after centrifugation (30 min.; 14,000× g; 4°C). Protein concentration was determined using a Bicinchoninic Acid Kit (Sigma-Aldrich).

Cytokine Expression-Protein Microarray

Analysis of cytokine expression was performed using an antibody array for human inflammation factors (ab134003; Abcam, UK). The assay was performed in accordance with the manufacturer's instructions. The membranes were visualised using a visible fluorescent Western blot imaging system (Azure Biosystems C400, Azure, USA) and analyzed using ImageJ software. The obtained results were normalised to the control dots. The assay was performed in accordance with the manufacturer's instructions using lysates containing 200 µg/mL of total protein per membrane.

Gene Expression

Isolation of Total RNA

For the isolation of total RNA, U87, U118, U251, and T98 cells (1×10^5 cells per well) were incubated for 24 h. Subsequently, the medium was removed, and GO-antisense miRNA-21 ($GO_{100\ \mu g/mL}$:$miRNA_{5\ pmol/mL}$) was added to the cells and incubated for an additional 24 h. Total RNA was isolated using an RNA Mini Kit (PureLink®, Ambion™ Life Technologies, Foster City, CA, USA). The resulting cell pellet was resuspended in a lysis buffer containing 1% 2-mercaptoethanol, and subsequently, the frozen metal balls were added to the probe and homogenised in a ball mill (TissueLyser, Qiagen, Germantown, MD, USA) for 5 min at 50 Hz. The homogenate was centrifuged at 12,000×g. The supernatant containing total RNA was transferred into a new tube, and one volume of 70% ethanol was added to each volume of cell homogenate, following the manufacturer's instructions. Total RNA was eluted in 50 µL RNase-free water and stored at −80°C. The isolated RNA was measured using a spectrophotometer (NanoDrop 2000, Thermo Scientific, Wilmington, DE, USA). The cDNA was synthesised with a cDNA High Capacity Reverse Transcription Kit (AppliedBiosystems, Foster City, CA, USA) to reverse-transcript the mRNA to cDNA using 2200 ng per reaction. The obtained cDNA was measured using a spectrophotometer and stored for further analysis at −20°C.

Real-Time PCR

The ΔΔCt method was used to determine the expression of mRNA using real-time PCR Equation (2):

$$\Delta\Delta CT = \Delta CT\ test\ sample - \Delta CT\ calibrator\ sample \tag{2}$$

.

The reaction was carried out using 48-well plates and a qPCR reagents kit (Luminaris Color HiGreen reagents qPCR Master Mix, Thermo Fisher Scientific); 100 ng of cDNA was used for each reaction. The following genes were examined: IL-8, TIMP-2, ICAM-1, and MCP-1. The primers used for this procedure are presented in Table 1.

Glyceraldehyde-3-phosphate dehydrogenase (GAPDH) was used as the reference housekeeping gene. The reaction conditions were set as specified by the manufacturer, and each sample was analysed in duplicate. The procedure was conducted using a real-time PCR system (StepOnePlus™). qPCR results were normalised to the control (Log2FC = 0). Relative expression was calculated using the GPDH gene and control group (0).

Statistical Analysis

Densitometry results from the protein array were analyzed by the unpaired one-way ANOVA. P-values that were < 0.05 were considered significant. The analyses were performed using GraphPad Prism (GraphPad Software, Inc. CA, USA). All mean values were presented with standard deviations.

Table 1 Primer Sequences Used for Real-Time Quantitative Reverse Transcriptase Polymerase Chain Reaction (qRT-PCR)

Gene	Forward	Reverse
IL-8	GAGAGTGATTGAGAGTGGACCAC	CACAACCCTCTGCACCCAGTTT
TIMP-2	ACCCTCTGTGACTTCATCGTGC	GGAGATGTAGCACGGGATCATG
ICAM-1	AGCGGCTGACGTGTGCAGTAAT	TCTGAGACCTCTGGCTTCGTCA
MCP-1	AGAATCACCAGCAGCAAGTGTCC	TCCTGAACCCACTTCTGCTTGG

Results

Transmission Electron Microscopy and Fourier Transform Infrared (FTIR) Spectrum

The ultrastructure of GO flakes, after functionalisation by antisense miRNA-7 observed by transmission electron microscopy showed a high affinity of antisense miRNA-21 into flake surfaces (Figure 1A and B) and did not cause agglomeration of miRNA sequences or GO. GO functionalisation involved the attachment of the antisense miRNA-21 oligonucleotide to the oxygen functional groups on the surface of the GO, but the analysis of the Fourier transform infrared (FTIR) spectrum (Figure 1C and D) showed that the interaction was based on non-covalent bonding. The FTIR spectrum of GO typically shows characteristic peaks associated with the functional groups present on its surface, including hydroxyl (-OH), carboxyl (-COOH), and epoxy (-C-O-) groups. The antisense miRNA-21 oligonucleotide, which is likely to be used to functionalize GO in this case, contains phosphate groups (-PO4) and nucleobases, which introduced additional spectral features shown in Figure 1F.

Dynamic Light Scattering, ζ-Potentials and Entrapment Efficiency

The size distribution (Figure 2) measured by the DLS method showed a high affinity of GO to the antisense miRNA-21, such that GO-antisense miRNA-21 performed as a stabile hydrocolloid with a polydispersity index (PDI) = 0.539. For GO and antisense miRNA-2 the polydispersity indexes were 0.585 and 0.995, respectively. The ζ-potential is a measure of the electrostatic potential at the surface of a particle or colloid. In the case of GO-antisense miRNA-21 complexes, the ζ-potential can provide important information on the stability and surface charge of the complex. The obtained results for the ζ-potential of GO and GO-antisense miRNA-21 were −10±2,78 mV, −12,5±2,04 mV, and −28,5±2,22mV, respectively. The Entrapment Efficiency results showed that the GO-antisense miRNA-21 complex had EE = 99.19%.

Cell Morphology and Transfection Efficiency Evaluation

The exposition of the U87, U118, U251, and T98 glioma cell lines on the GO, GO-antisense miRNA-21, and antisense miRNA-21 caused several morphological changes, including shortened cytoplasmic tentacles and reduced size of cells, which indicated the stressful environment, but also verified the transfection efficiency (Figure 3).

Cell Viability

The cell viability of the U87, U118, U251, and T98 glioma cell lines was evaluated by the metabolic activity of cells after GO, GO-antisense miRNA-21, and antisense miRNA-21 treatment (Figure 4).

Cytokine Expression - Protein Expression Level

The cytokine profile assessment by microarrays showed that the electroporation and GO-based delivery of antisense miRNA-21 caused an increase in the protein level of interleukin 6 (IL-6), interleukin 8 (IL-8), interleukin 10 (IL-10), intercellular adhesion molecule 1 (ICAM-1), monocyte chemoattractant protein-1 (MCP-1), and metallopeptidase inhibitor 2 (TIMP-2) at the U87, U118, U251, and T98 cell lines (Figures 5 and 6).

Cytokine Expression - Gene Expression

Electroporation, compared to GO-based delivery of antisense miRNA-21 into glioma cells, caused a significant increase in the protein level of interleukin 6 (IL-6), interleukin 8 (IL-8), intercellular adhesion molecule 1 (ICAM-1), and

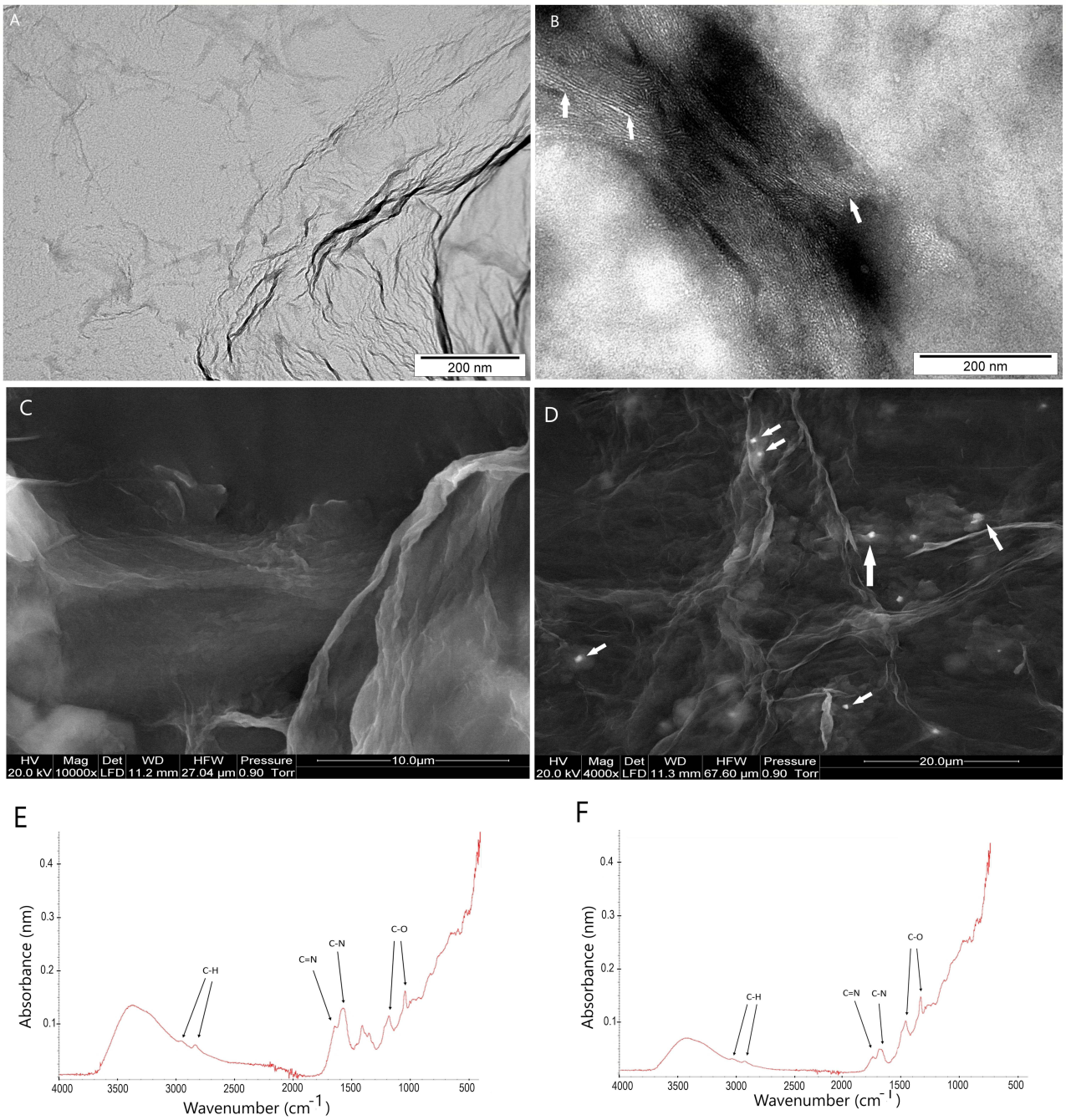

Figure 1 Transmission (TEM) and scanning electron microscopy (SEM) images of (**A**–**C**) graphene oxide and (**B**–**D**) graphene oxide–antisense miRNA-21 complex and FITR spectrum of (**E**) graphene oxide and (**F**) graphene oxide–antisense miRNA-21 complex. White arrows point to the antisense miRNA-21 strand. Scale bars: 200nm-20µm. The FITR spectra were triplicated per each sample.

monocyte chemoattractant protein-1 (MCP-1) (Figure 7). The GO-based antisense miRNA-21 transfection caused an increased level of metallopeptidase inhibitor 2 (TIMP-2). IL-6, as an inflammatory cytokine, regulates the inflammatory reaction and increased cell proliferation and angiogenesis in cancer cells. The densitometry analysis of obtained microarray protein membranes showed that the expression level of IL-8 was increased after delivery of antisense miRNA-21 into glioma cells, but electroporation was a significant cause. The qPCR analysis also showed that IL-8 was downregulated significantly compared to the non-treated control group after administration of GO, GO-antisense miRNA-21, or antisense miRNA-21 to the U251 glioma cell line. The mRNA expression level was also significantly

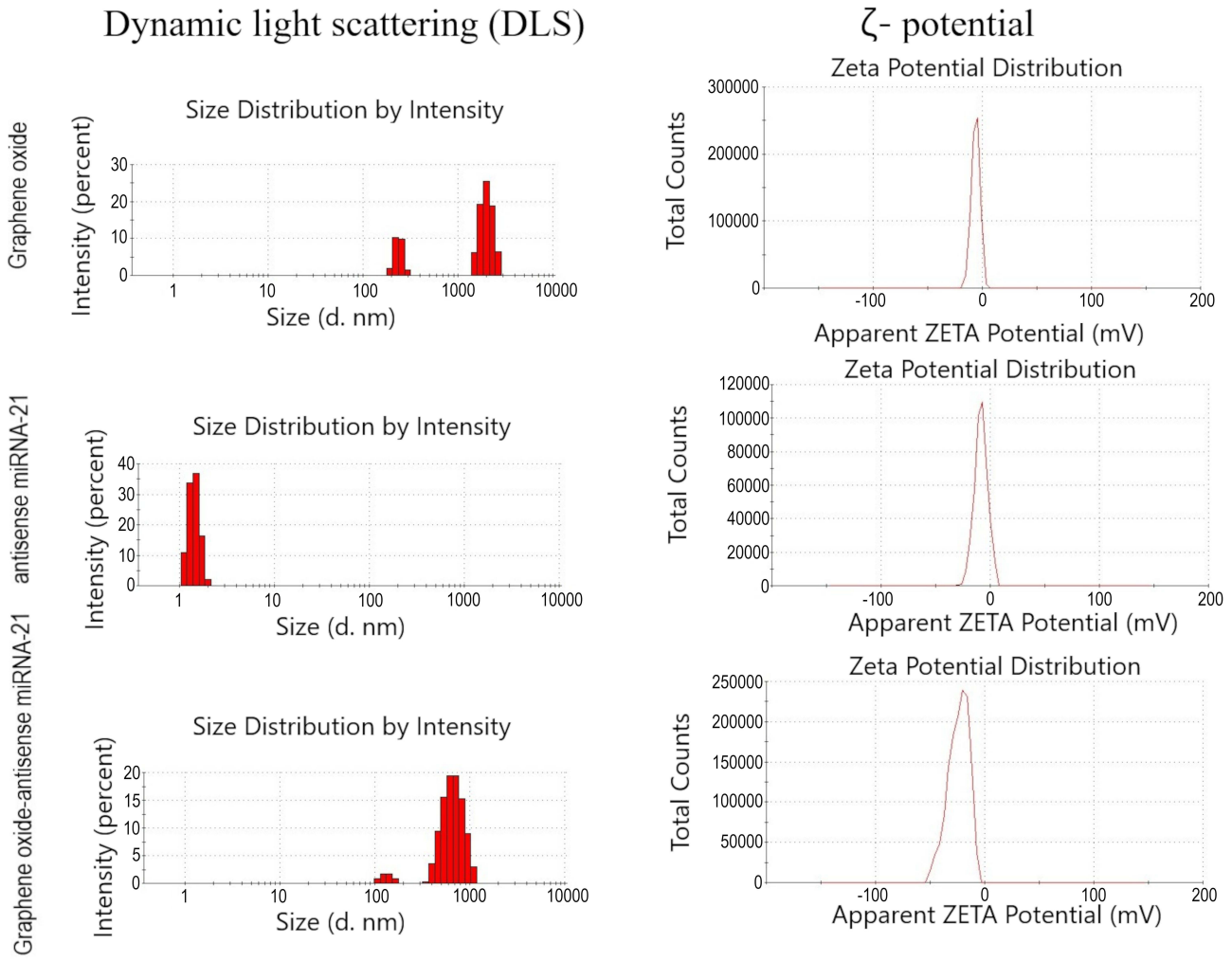

Figure 2 DLS and ζ-potential of graphene oxide, antisense miRNA-21, and complexes of graphene oxide-antisense miRNA-21. The DLS ζ-potential measurement was triplicated for each sample.

downregulated after the administration of GO to the U118 cell line. The obtained results showed that there were no differences in the gene expression level of IL-8 at the U87 cell line.

Discussion

Gliomas are one of the deadliest types of central nervous cancers, as they have great resistance to standard treatment. Over the last decade, there has been an increased interest in cancer gene therapy due to the possibility of overcoming the poor prognosis for patients diagnosed with glioma. The small non-coding sequences of miRNA are highly deregulated in gliomas, so the possibility of regulating the proper level of its expression in glioma becomes an interesting proposition. Selected miRNA sequences in glioma can be inhibited by direct and indirect inhibitors. miRNA inhibitors delivered as an antisense sequence into cancer tissue have shown low toxicity and high efficiency at gene knock-down.[12] However, the possible side effects of using viral vectors[1] and miRNA's poor stability led to a need for an alternative method of delivering nucleotide sequences into cancer cells. In the last decade, many efforts have been directed toward nanobiotechnology and carbon nanomaterials. GO, as a single carbon atom layer, has unique physicochemical properties which affect GO's bioactivity against glioma cell lines. The high affinity of GO to nucleic acids is attributed to its unique properties, including a large surface area and the presence of oxygen-containing functional groups on its surface. These properties allow GO to bind to nucleic acids through electrostatic interactions, hydrogen bonding, and π-π stacking. In our studies the FTIR spectra results indicated that the chemical connection between the surface of GO and antisense

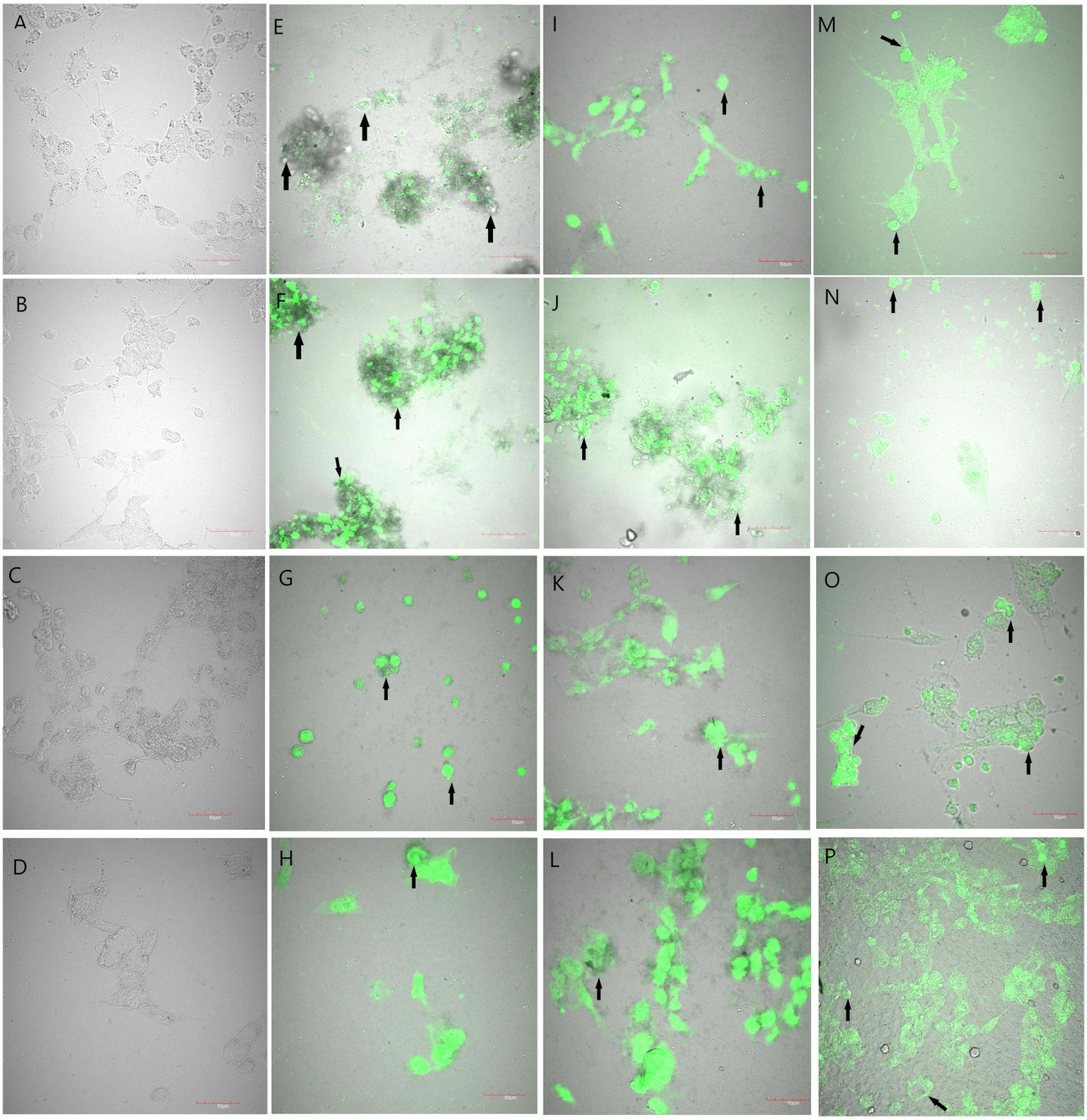

Figure 3 Morphology of U87 (**A, E, I** and **M**), U118 (**B, F, J** and **N**), U251 (**C, G, K** and **O**), and T98 (**D, H, L** and **P**) glioma cell lines treated with graphene oxide conjugated with FITC (**E–H**), graphene oxide–antisense miRNA-21 conjugated with FITC (**I–L**) and antisense miRNA-21 conjugated with FITC (**M–P**). Control group (non-treated cells): U87 (**A**), U118 (**B**), U251 (**C**), and T98 (**D**). Confocal microscopy. Scale bars: 50μm.
Abbreviation: FITC, fluorescein isothiocyanate.

miRNA-21 was not detected. Moreover, the evaluation of C/O ratio of GO after functionalization with antisense miRNA-21 will verify the changes in the C and O atoms content resulting from the functionalization process. The self-organisation of GO flakes under the influence of nucleotides has been extensively used in drugs, small molecules of nucleotides delivery.[13] GO flakes were arranged at the nanoscale for nanomaterials, but except for the size, the PDI index verified the level of functionalisation of GO. Generally, the PDI is a measure of the size distribution of particles or molecules in a sample. A PDI value of 0 indicates a monodisperse sample, while a PDI value closer to 1 indicates a more polydisperse sample. The relatively low PDI values for GO-antisense miRNA-21 complexes suggest that the complexes

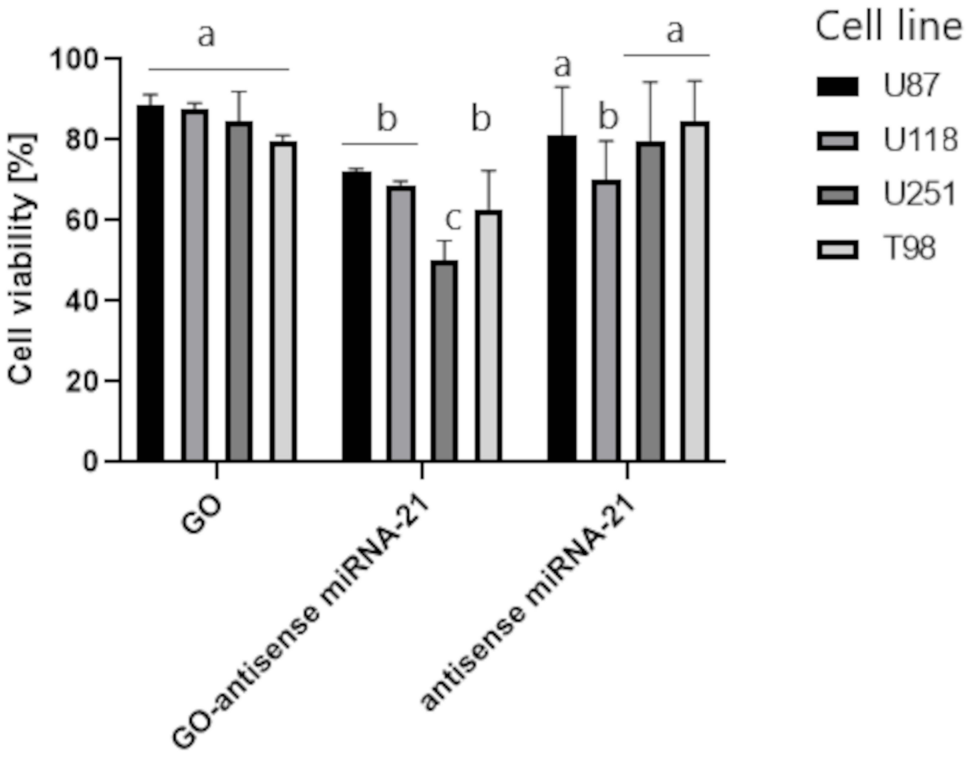

Figure 4 U87, U118, U251 and T98 cell viability. [a,b,c]$p<0.05$. The data present an average from triplicated measurements for each sample.
Abbreviations: GO, graphene oxide, GO-antisense miRNA-21, graphene oxide complex with antisense miRNA-21.

are relatively uniform in size and shape, which can be important for their stability, drug loading, and biological activity. However, it is important to note that PDI can be influenced by a variety of factors, including the preparation method, the concentration of the complex, and the characteristics of the surrounding medium. The functionalisation of GO by antisense miRNA-21 can also be described by differences in ζ-potential between GO and GO-antisense miRNA-21. Compared to our obtained results, GO-antisense walR complexes showed a ζ-potential of 33.7 mV, which indicated that the complexes were positively charged and stable in solution.[32] Another published result of ζ-potential for GO-PEG complexes with miR-29b was 43 ± 1.33 mV, indicating that the complexes were negatively charged but also stable in solution. The negative ζ-potential of GO-antisense miRNA-21 complexes is due to the presence of negatively charged oxygen-containing functional groups on the surface of GO and the negatively charged phosphate backbone of the nucleic acid. This negative charge can prevent aggregation and stabilise the complex in the solution. Moreover, if GO is dispersed in a liquid medium, the presence of negatively charged surface charges can be balanced by the presence of positively charged counterions in the solution or culture medium and can be efficiently loaded by negatively charged antisense miRNA-21. Moreover, the high EE index of GO-antisense miRNA-21 complexes refers to the high percentage of antisense miRNA-21, which means that antisense miRNA-21 sequences were effectively trapped or encapsulated within the GO structure during the delivery process. Several studies have reported high entrapment efficiencies for GO-based drug delivery systems. For example, already published data reported an entrapment efficiency of 39.98 ± 7.63% for the anticancer drug doxorubicin using a GO-based nanocarrier.[33] Another study showed 83% entrapment efficiency of GO functionalised by methotrexate.[34] In our study, the EE was higher compared to the mentioned studies and indicated that antisense miRNA-21 was deposited with high affinity on GO flakes. However, the EE of GO can vary depending on various factors, such as the method of preparation, the size and concentration of the drug molecule, and the properties of the surrounding medium.

The effectiveness of the functionalisation can also be described by tracking the uptake of fluorescent dye. The increased level of FITC fluorescent insensitivity indicated that the transfection of glioma cells was efficient and indicated that GO-antisense miRNA-21 showed a high level of selectivity compared to antisense miRNA-21 delivered by

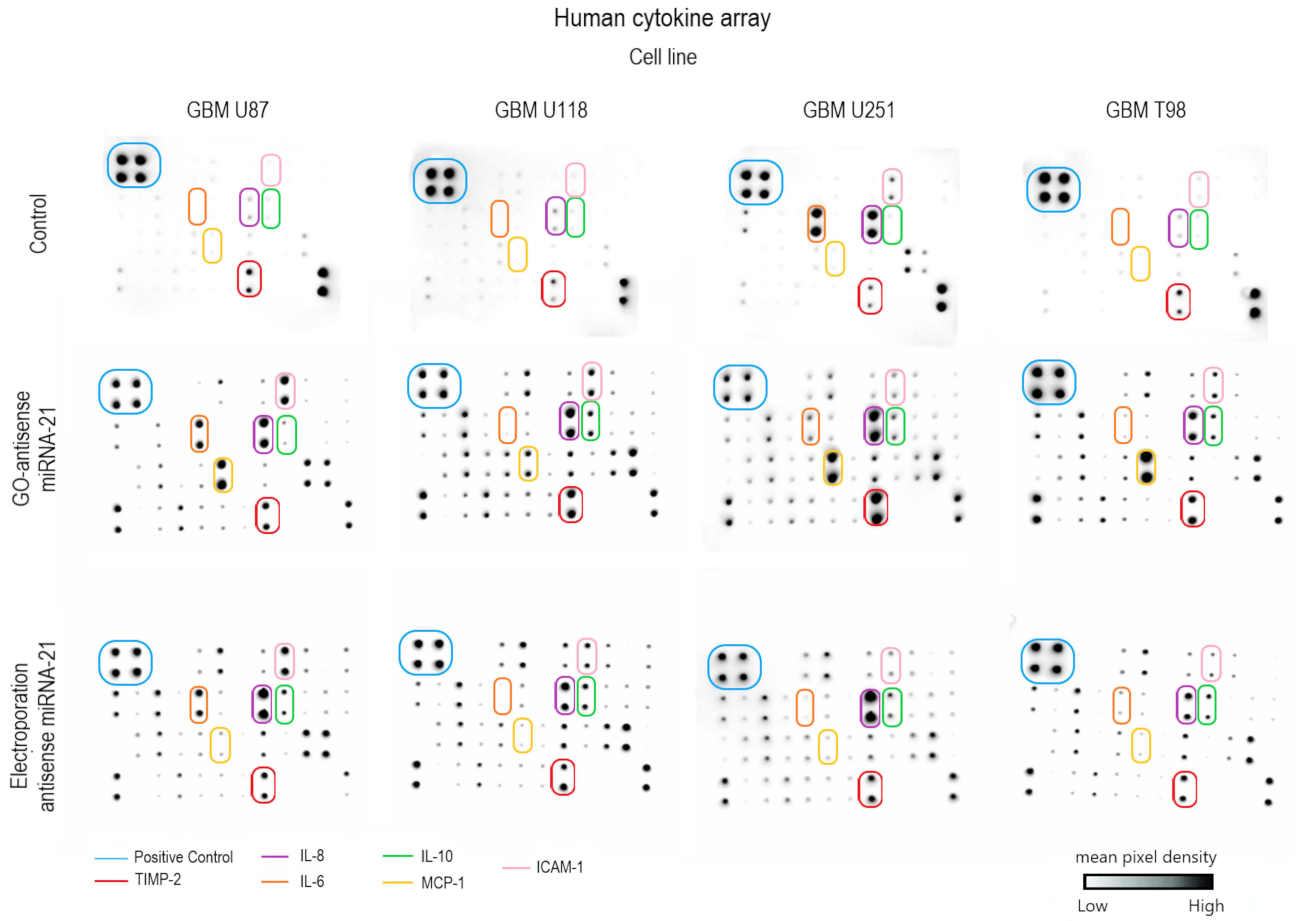

Figure 5 Cytokine antibody array. Control – non-treated glioblastoma cell line. Glioblastoma cell line: U87, U118, U251, and T98. The arrows point to significantly changed pixel densities of positive dots of protein: interleukin 6 (IL-6), interleukin 8 (IL-8), interleukin 10 (IL-10), intercellular adhesion molecule 1 (ICAM-1), monocyte chemoattractant protein-1 (MCP-1), and metallopeptidase inhibitor 2 (TIMP-2).

electroporation. This method is simple and fast for tracking the biodistribution of nanomaterials under in vitro and in vivo conditions.[35] The results of viability showed that at U87, U118, U251, and T98 investigated cell lines the cytotoxic effect was observed after GO administration. However, the highest reduction level of cell viability was observed after GO-antisense miRNA-21 administration. Based on the literature the cytotoxic effect of GO-containing materials can be assigned to the extremely sharp edges of graphene and cell wall membrane damage,[27] ROS generation[28] and trapping the cells within the aggregated graphene sheets.[29] The obtained results confirmed already published data, where GO-antisense miRNA-21 complex targeting miRNA-21 was found to effectively reduce the expression of miRNA-21 in cancer cells and inhibit their proliferation and migration.[30,31] Moreover, our studies showed that GO-antisense miRNA-21 could modify the inflammatory response by affecting the cytokine expression level. IL-6, as an inflammatory cytokine, regulates the inflammatory reaction and increased cell proliferation and angiogenesis in cancer cells. The tumour microenvironment can produce cytokines/chemokines, which are involved in the recruitment of normal cells to promote growth, invasion, angiogenesis, and metastasis of glioblastoma.[36] The exact cytokines that are secreted from glioblastoma tissue may vary depending on the specific case and the stage of the disease. A high level of IL-6 expression corresponds with a higher grade of glioma and increased invasiveness, metastasis, and reprogramming of the tumour microenvironment.[25] Interleukin-8 (IL-8) is a chemokine that plays a role in angiogenesis, inflammation, and tumour growth. In glioma, IL-8 is known to be overexpressed and has been implicated in the promotion of tumour growth and invasion.[22] One of the main ways that IL-8 affects glioma is through its ability to stimulate angiogenesis. Gliomas require a blood supply to grow and spread, and IL-8 promotes the formation of new blood vessels to supply the tumour with nutrients and oxygen. This can lead to increased tumour growth and invasiveness. IL-8 also plays a role in inflammation,

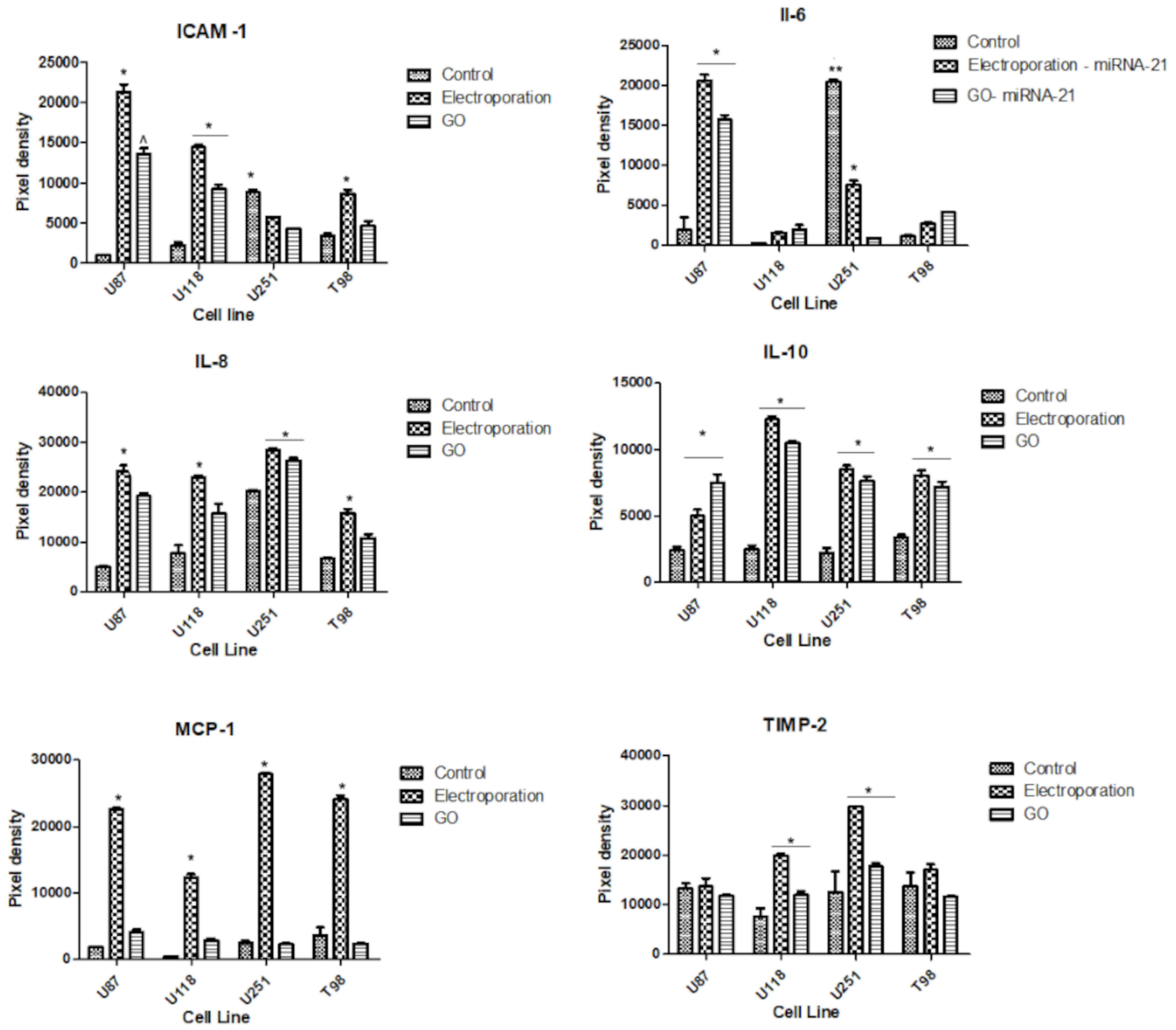

Figure 6 Summary of protein arrays dots pixels densitometry analysis of intercellular adhesion molecule 1 (ICAM-1), interleukin 6 (IL-6), interleukin 8 (IL-8), interleukin 10 (IL-10), monocyte chemoattractant protein-1 (MCP-1), and metallopeptidase inhibitor 2 (TIMP-2). ***^p ≤ 0.05. The data present an average from triplicated measurements for each sample.
Abbreviation: GO, graphene oxide.

which is thought to contribute to the development and progression of glioma. Wierzbicki et al[37] published data where the regulation of IL-8 and the expression level of IL-6 was downregulated at the U87 but not at the U118 cell line and corresponds to the silencing of NF-κB signalling pathways after administration of carbon allotropes. In the aforementioned study, the downregulation of the NF-κB protein expression level indicated the antiangiogenic properties of nano-sized graphene oxide. According to the Cancer Genome Atlas and Ivy Glioblastoma Atlas Project[38] data, IL-8 expression is negatively correlated with glioma patient survival. Moreover, IL-8 stimulates angiogenesis and tumour progression in glioma, and it is a key microenvironmental factor involved in promoting a switching of the cellular polarity in glioma. Increased IL-6 and IL-8 expression levels stimulate proangiogenic factors in glioma and promote tumour cell proliferation. A high level of IL-6 affects MMP activity and decreases the protein expression of MHC II, CD80, and CD60 in glioma. It is worth noting that the obtained results showed that electroporation with antisense miRNA-21 significantly increased the expression of IL-6, IL-8 and IL-10, but GO-based transfection with antisense miRNA-21 showed a cell-dependent effect, and at U118 and T98 the differences in protein expression were insignificant compared with the control

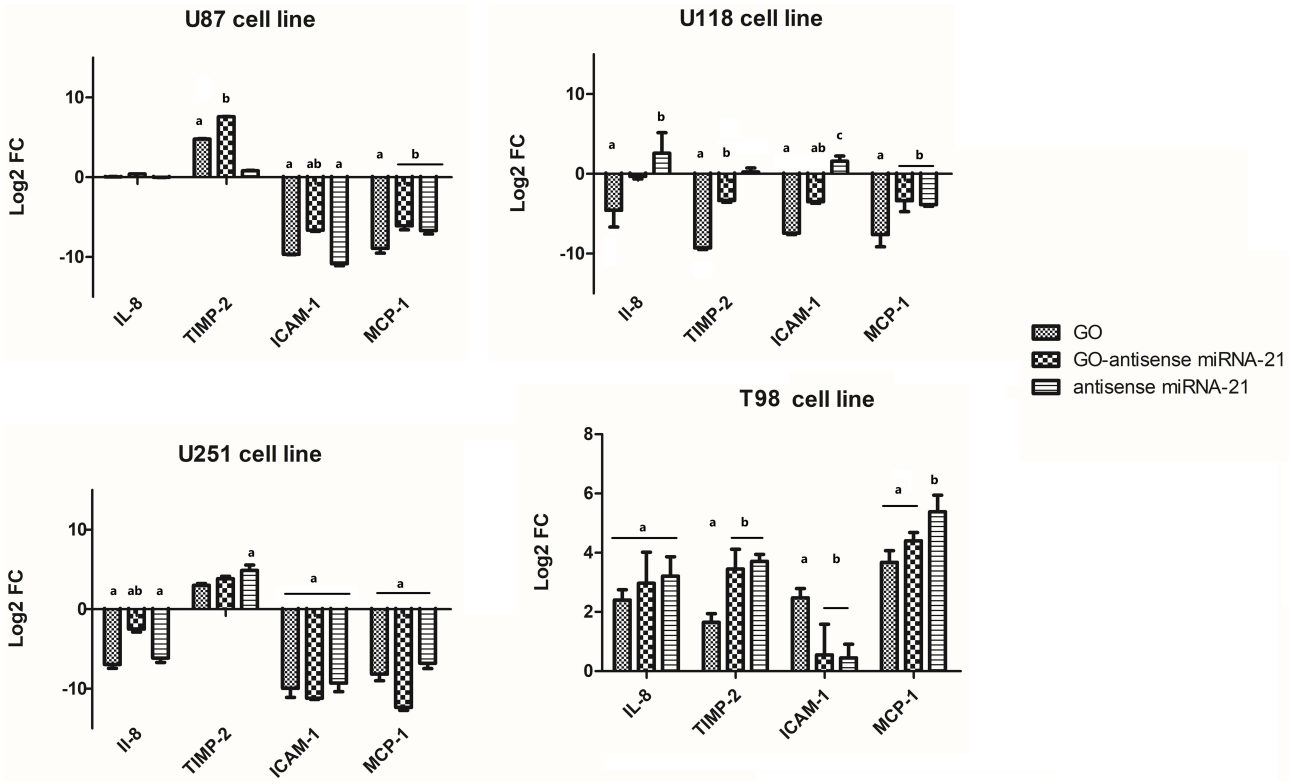

Figure 7 Expression of genes IL-8, TIMP-2, ICAM-1, and MCP-1 at the mRNA level in U87, U118, U251, and T98 glioblastoma cells 24 h after administration of graphene oxide (GO), a complex of graphene oxide with antisense miRNA-21 (GO-antisense miRNA-21), and antisense miRNA-21 using RT-PCR. Bars represent means with standard deviation (SD) (n = 3). Relative expression was calculated using the *gapdh* gene and the control group (0). The results are presented as log2FC values. Values above/below 0 indicate upregulation/downregulation of gene expression.

Notes: Different lowercase letters (a, b, c) within columns indicate significant differences between the miRNA ($p \leq 0.05$). The data present an average from triplicated measurements for each sample.

Abbreviation: FC, fold change.

non-treated cancer cell lines. Elucidating the mechanism of cytokine release from glioma cells after electroporation can be based on the selection of the antisense miRNA-21 transfection method. Wierzbicki et al[37] showed that nano-sized GO treatment of the U87 and U118 glioma cell lines leads to a decrease in IL-6 and IL-8 protein expression levels. Electroporation, in our preliminary study, showed significant side effects on glioma cell lines. It increased the secretion of cytokines involved in tumour proliferation, metastasis, and resistance to chemotherapy. The administration of GO and GO-antisense miRNA-21 showed that the expression level of TIMP-2 was significantly upregulated at the U87, U251, and T98 glioma cell lines but not at the U118 cell line. TIMP-2 is a tissue inhibitor of metalloproteinases, which are enzymes that can degrade extracellular matrix proteins and promote the invasion and metastasis of cancer cells. TIMP-2 can inhibit the activity of metalloproteinases and limit their ability to promote invasion in glioma. The expression of TIMP-2 can be modulated by physiochemical and physical conditions.[39] The expression level of TIMP-2 protein also depends on the type of cancer cells and is correlated with the malignancy of cancer. Lu et al[40] suggest that glioma cells can stimulate the activation of MMP-2 by endogenous TIMP-2 concentrations; however, an increased level of local TIMP-2 inhibits MMP-2 activity. This inhibition is based on a complex model involving the indirect binding of TIMP-2 to MT1-MMP, which downregulates the amount of TIMP-free MT1-MMP molecules available for proMMP-2 cleavage, and the direct binding of TIMP-2 to proMMP-2 leads, sequestering the TIMP-2 from the activation complex.[32] Our results showed that the expression level of TIMP-2 after administration of GO, GO-antisense miRNA-21 or antisense miRNA-21 was cell type dependent and probably depends on the physiological activity of the glioma cell and its metastasis activity. At U118, the expression level of TIMP-2 was significantly decreased compared to the control group, which pointed to the indirect binding of TIMP-2 and the reduction of free TIMP-2 level in the cell. Moreover, the U87, U118, U251, and T98 glioma cell lines have different abilities to invade and migrate and have different expressions of

specific proteins, such as EGFR and MMP-2, which play a role in glioma cell growth and invasion. On the other hand, IL-6 regulates the inflammatory reaction and increased cell proliferation and angiogenesis in cancer cells. A high level of IL-6 expression corresponds with a higher grade of glioma and increased invasiveness, metastasis, and reprogramming of the tumour microenvironment. One of the main mechanisms by which IL-6 affects glioma is through its ability to promote inflammation. Gliomas are known to be infiltrated by immune cells and cytokines, and IL-6 is one of the cytokines that is overexpressed in glioma tissue. IL-6 can stimulate the immune system and promote inflammation, which can contribute to the development and progression of glioma. IL-6 can also promote the growth and survival of glioma cells. It can activate signalling pathways that lead to increased cell proliferation and survival, and it can also regulate the expression of genes involved in cell cycle progression and apoptosis. A higher level of IL-8 expression can also stimulate the activation of ICAM-1, which increases glioma's resistance to antiangiogenic therapy.[41] ICAM-1 is a molecule that is involved in cell adhesion and can promote interaction between immune cells and cancer cells. ICAM-1 has been shown to be overexpressed in glioma and can promote invasion and metastasis by facilitating interaction between cancer cells and the surrounding tissue. ICAM-1 overexpression was detected in various cell types, including human cancer cells, eg, lung, breast, prostate, or glioma. The obtained result in our studies showed that the protein expression of ICAM-1 also had a cell-dependent effect after delivery of antisense miRNA-21 into glioma cell lines. The highest reduction of ICAM-1 protein expression level was observed in the U251 and T98 glioma cell lines, compared to the non-treated glioma cell lines. Moreover, electroporation with antisense miRNA-21 caused increased expression at all investigated glioma cell lines. In glioma, overexpression of ICAM-1 was observed at higher grades, promoting invasion and metastases, leading to resistance to antiangiogenic therapy, and indirectly affecting the TIMP/RECK pathway.[42] Glioma cells generate different types of chemokines and their receptors, which are involved in various biological aspects of glial tumours, such as invasiveness, survival, angiogenesis, and proliferation. MCP-1 is generated by glioma cells under oxidative stress or high expression levels of growth factors.[43] Monocytes are essential for the initiation of tumour neovascularisation due to their adherence to and invasion of the endothelium. In glioma, MCP-1 can stimulate the migration and invasion of cancer cells and exert its paracrine effects on the tumour microenvironment.[43] Our obtained results showed that the MCP-1 protein expression level was significantly increased after electroporation with antisense miRNA-21 compared to the control non-treated glioma cells but also compared to the GO-based transfection. IL-8 and MCP-1 are both chemokines that can promote angiogenesis, inflammation, and tumour growth in glioma. The published data also point to the possibility of interactions between IL-8 and MCP-1, which have been found to be upregulated in cancer tissue, and their expression has been correlated with the expression of TIMP-2 and ICAM-1.[44] This suggests that there may be crosstalk between these molecules in the regulation of glioma growth and invasion. The inhibition of miR-21 by antisense miR-21 can affect the expression of TIMP-2 and ICAM-1 in glioma cells and cause its downregulation. During our research, obtained data pointed to the possibility of inhibiting miR-21 with antisense miR-21 in glioma cells leading to the increased expression of TIMP-2 and the decreased expression of ICAM-1 associated with decreased invasion and migration of glioma cells.

It is important to note that the effects of GO complexes with antisense miRNA-21 depend on the type of the treated cell and tissue, the dose and duration of exposure, and also the chemical composition of the GO complex. The results of this study suggest the effectiveness of the transfection method for future investigation of the direct role of antisense miRNA-21 against glioma tumours. Moreover, the assessment of the cytokine expression profile indicates that the GO-antisense miRNA-21 can be beneficial and can change the cytokine expression level in glioblastoma cells and reduce cell viability.

Conclusions

Graphene oxide (GO) with antisense miRNA-21 as a complex affected the cytokine expression level and decreased MCP-1 and TIMP-2 cytokine expression levels compared to the electroporation process of delivery of antisense miRNA-21 into glioma cell lines. Thus, the possibility of delivering antisense miRNA-21 by GO surface and, at the same time, reducing the cytokine secretion from glioma cells by GO-miRNA-21 complexes is a very optimistic proposal for future investigations.

Acknowledgments

This work was supported by the Polish National Research Council grant NCN 2016/23/D/NZ7/03837. The manuscript is part of the habilitation thesis of Marta Kutwin.

Disclosure

The authors report no conflicts of interest in this work.

References

1. Dranoff G, Mulligan RC. Gene transfer as cancer therapy. *Adv Immunol*. 1995;58:417–454.
2. Zhang WW, Li L, Li D, et al. The first approved gene therapy product for cancer Ad-p53 (Gendicine): 12 years in the clinic. *Hum Gene Ther*. 2018;29(2):160–179. doi:10.1089/hum.2017.218
3. Lee YS, Dutta A. MicroRNAs in cancer. *Annu Rev Pathol*. 2009;4(1):199–227. doi:10.1146/annurev.pathol.4.110807.092222
4. Ganju A, Khan S, Hafeez BB, et al. miRNA nanotherapeutics for cancer. *Drug Discov Today*. 2017;22(2):424–432. doi:10.1016/j.drudis.2016.10.014
5. Esteghamat A, Akhavan O. Graphene as the ultra-transparent conductive layer in developing the nanotechnology-based flexible smart touchscreens. *Microelectronic Eng*. 2022;2022:111899.
6. Olabi AG, Abdelkareem MA, Wilberforce T, Sayed ET. Application of graphene in energy storage device–A review. *Renew Sust Energ Rev*. 2021;135:110026.
7. Jalilinejad N, Rabiee M, Baheiraei N, et al. Electrically conductive carbon-based (bio)-nanomaterials for cardiac tissue engineering. *Bioeng Transl Med*. 2022;8(1):e10347. doi:10.1002/btm2.10347
8. Wu X, Hu J, Qi J, Hou Y, Wei X. Graphene-supported ordered mesoporous composites used for environmental remediation: a review. *Sep Purif Technol*. 2020;239:116511. doi:10.1016/j.seppur.2020.116511
9. Wang Y, Li Z, Wang J, Li J, Lin Y. Graphene and graphene oxide: biofunctionalization and applications in biotechnology. *Trends Biotechnol*. 2011;29(5):205–212. doi:10.1016/j.tibtech.2011.01.008
10. Mendonca MC, Soares ES, de Jesus MB, et al. Reduced graphene oxide induces transient blood–brain barrier opening: an in vivo study. *J Nanobiotechnol*. 2015;13(1):78. doi:10.1186/s12951-015-0143-z
11. Priyadarsini S, Mohanty S, Mukherjee S, Basu S, Mishra M. Graphene and graphene oxide as nanomaterials for medicine and biology application. *J Nanostructure Chem*. 2018;8(2):123–137. doi:10.1007/s40097-018-0265-6
12. Kutwin M, Sosnowska ME, Strojny-Cieślak B, et al. MicroRNA delivery by graphene-based complexes into glioblastoma cells. *Molecules*. 2021;26(19):5804. doi:10.3390/molecules26195804
13. Liu J, Cui L, Dusan L. Graphene and graphene oxide as new nanocarriers for drug delivery applications. *Acta Biomaterialia*. 2013;9(12):9243–9257. doi:10.1016/j.actbio.2013.08.016
14. Akhavan O, Ghaderi E. Toxicity of graphene and graphene oxide nanowalls against bacteria. *ACS Nano*. 2010;10(10):5731–5736. doi:10.1021/nn101390x
15. Veliev F, Briançon-Marjollet A, Bouchiat V, Delacour C. Impact of crystalline quality on neuronal affinity of pristine graphene. *Biomaterials*. 2016;86:33–41. doi:10.1016/j.biomaterials.2016.01.042
16. Hinzmann M, Jaworski S, Kutwin M, et al. Nanoparticles containing allotropes of carbon have genotoxic effects on glioblastoma multiforme cells. *Int J Nanomedicine*. 2014;9:2409–2417. doi:10.2147/IJN.S62497
17. Akhavan O, Ghaderi E, Akhavan A. Size-dependent genotoxicity of graphene nanoplatelets in human stem cells. *Biomaterials*. 2012;33(32):8017–8025. doi:10.1016/j.biomaterials.2012.07.040
18. Kurantowicz N, Strojny B, Sawosz E, et al. Biodistribution of a high dose of diamond, graphite, and graphene oxide nanoparticles after multiple intraperitoneal injections in rats. *Nanoscale Res Lett*. 2015;10(1):39817. doi:10.1186/s11671-015-1107-9
19. Vogel TW, Zhuang Z, Li J, et al. Proteins and protein pattern differences between glioma cell lines and glioblastoma multiforme. *Clin Cancer Res*. 2005;11(10):3624–3632. doi:10.1158/1078-0432.CCR-04-2115
20. Aloizou AM, Pateraki G, Siokas V, et al. The role of MiRNA-21 in gliomas: hope for a novel therapeutic intervention? *Toxicol Rep*. 2020;6(7):1514–1530. doi:10.1016/j.toxrep.2020.11.001
21. Pfeffer SR, Yang CH, Pfeffer LM. The Role of miR-21 in Cancer. *Drug Dev Res*. 2015;76(6):270–277. doi:10.1002/ddr.21257
22. Zhang H, Li J, Li G, Wang S. Effects of celastrol on enhancing apoptosis of ovarian cancer cells via the downregulation of microRNA-21 and the suppression of the PI3K/Akt-NF-κB signaling pathway in an in vitro model of ovarian carcinoma. *Mol Med Rep*. 2016;14(6):5363–5368. doi:10.3892/mmr.2016.5894
23. Pandit A, Begum Y, Saha P, Srivastava AK, Swarnakar S. Approaches toward targeting matrix metalloproteases for prognosis and therapies in gynecological cancer: microRNAs as a molecular driver. *Front Oncol*. 2022;25(11):720622. doi:10.3389/fonc.2021.720622
24. Ravid Y, Formanski M, Smith Y, Reich R, Davidson B. Uterine leiomyosarcoma and endometrial stromal sarcoma have unique miRNA signatures. *Gynecol Oncol*. 2016;140(3):512–517. doi:10.1016/j.ygyno.2016.01.001
25. Borzooee Moghadam N, Avatefi M, Karimi M, Mahmoudifard M. Graphene family in cancer therapy: recent progress in cancer gene/drug delivery applications. *J Mater Chem B*. 2023;11(12):2568–2613. doi:10.1039/d2tb01858f
26. Hwang DW, Kim HY, Li F, et al. In vivo visualization of endogenous miR-21 using hyaluronic acid-coated graphene oxide for targeted cancer therapy. *Biomaterials*. 2017;121:144–154. doi:10.1016/j.biomaterials.2016.12.028
27. Hu W, Peng C, Lv M, et al. Protein Corona-mediated mitigation of cytotoxicity of graphene oxide. *ACS Nano*. 2011;5(5):3693–3700. doi:10.1021/nn200021j
28. Liao KH, Lin YS, Macosko CW, Haynes CL. Cytotoxicity of graphene oxide and graphene in human erythrocytes and skin fibroblasts. *ACS Appl Mater Interfaces*. 2011;3(7):2607–2615. doi:10.1021/am200428v

29. Hashemi E, Akhavan O, Shamsara M, Rahighi R, Esfandiar A, Tayefeh AR. Cyto and genotoxicities of graphene oxide and reduced graphene oxide sheets on spermatozoa. *RSC Adv*. 2014;4(52):27213–27223. doi:10.1039/c4ra01047g
30. Paulmurugan R, Ajayan PM, Liepmann D, Renugopalakrishnan V. Intracellular microRNA quantification in intact cells: a novel strategy based on reduced graphene oxide based fluorescence quenching. *MRS Commun*. 2018;3(3):642–651. doi:10.1557/mrc.2018.120
31. Genedy HH, Delair T, Montembault A. Chitosan based microRNA nanocarriers. *Pharmaceuticals*. 2022;15(9):1036. doi:10.3390/ph15091036
32. Wu S, Liu Y, Zhang H, Lei L. Nano-graphene oxide with antisense walR RNA inhibits the pathogenicity of Enterococcus faecalis in periapical periodontitis. *J Dent Sci*. 2020;15(1):65–74. doi:10.1016/j.jds.2019.09.006
33. Zainal-Abidin MH, Hayyan M, Ngoh GC, Wong WF. Doxorubicin loading on functional graphene as a promising nanocarrier using ternary deep eutectic solvent systems. *ACS Omega*. 2020;5(3):1656–1668. doi:10.1021/acsomega.9b03709
34. Chai D, Hao B, Hu R, et al. Delivery of oridonin and methotrexate via PEGylated graphene oxide. *ACS Appl Mater Interfaces*. 2019;11(26):22915–22924. doi:10.1021/acsami.9b03983
35. Li J, Tian J, Yin H, et al. Chemical conjugation of FITC to track silica nanoparticles in vivo and in vitro: an emerging method to assess the reproductive toxicity of industrial nanomaterials. *Environ Int*. 2021;152:106497. doi:10.1016/j.envint.2021.106497
36. Dudek I, Skoda M, Jarosz A, Szukiewicz D. The molecular influence of graphene and graphene oxide on the immune system under in vitro and in vivo conditions. *Arch Immunol Ther Exp*. 2016;3(3):195–215. doi:10.1007/s00005-015-0369-3
37. Wierzbicki M, Sawosz E, Strojny B, Jaworski S, Grodzik M, Chwalibog A. NF-κB-related decrease of glioma angiogenic potential by graphite nanoparticles and graphene oxide nanoplatelets. *Sci Rep*. 2018;8(1):14733. doi:10.1038/s41598-018-33179-3
38. Hasan T, Caragher SP, Shireman JM, et al. Interleukin-8/CXCR2 signaling regulates therapy-induced plasticity and enhances tumorigenicity in glioblastoma. *Cell death disease*. 2019;10(4):292 . doi:10.1038/s41419-019-1387-6
39. Stetler-Stevenson WG, Brown PD, Onisto M, Levy AT, Liotta LA. Tissue inhibitor of metalloproteinases-2 (TIMP-2) mRNA expression in tumor cell lines and human tumor tissues. *J Biol Chem*. 1990;265(23):13933–13938. doi:10.1016/S0021-9258(18)77438-3
40. Lu KV, Jong KA, Rajasekaran AK, Cloughesy TF, Mischel PS. Upregulation of tissue inhibitor of metalloproteinases (TIMP)-2 promotes matrix metalloproteinase (MMP)-2 activation and cell invasion in a human glioblastoma cell line. *Lab Invest*. 2004;84(1):8–20. doi:10.1038/sj.labinvest.3700003
41. Piao Y, Henry V, Tiao N, et al. Targeting intercellular adhesion molecule-1 prolongs survival in mice bearing bevacizumab-resistant glioblastoma. *Oncotarget*. 2017;8(57):96970–96983. doi:10.18632/oncotarget.18859
42. Kesanakurti D, Chetty C, Rajasekhar Maddirela D, Gujrati M, Rao JS. Essential role of cooperative NF-κB and Stat3 recruitment to ICAM-1 intronic consensus elements in the regulation of radiation-induced invasion and migration in glioma. *Oncogene*. 2013;32(43):5144–5155. doi:10.1038/onc.2012.546
43. Lindemann C, Marschall V, Weigert A, Klingebiel T, Fulda S. Smac mimetic-induced upregulation of CCL2/MCP-1 triggers migration and invasion of glioblastoma cells and influences the tumor microenvironment in a paracrine manner. *Neoplasia*. 2015;17(6):481–489. doi:10.1016/j.neo.2015.05.002
44. Tamai S, Ichinose T, Tsutsui T, et al. Tumor microenvironment in glioma invasion. *Brain Sci*. 2022;12(4):505. doi:10.3390/brainsci12040505